Finite Deformation Modeling of Crystalline Defects in Hyper-elastic Material

Akihiro Nakatani[1,*], **Mitsuhiro Akita**[1]

[1] Department of Adaptive Machine Systems, Osaka University, Suita, Osaka 565-0871, Japan
[*] Corresponding author: nakatani@ams.eng.osaka-u.ac.jp

Abstract An updated Lagrangian formulation is established to deal with the finite deformation of hyper-elastic body including the discontinuous slips due to the nucleation of lattice defects. The principle of virtual power is modified to treat the discontinuous deformation measured by initial lattice and a computational model is established by a penalty method with Lagrange multiplier. A few examples are shown for the application of geometrically non-linear deformation of hyper-elastic body including some dislocation structures and they are compared with the solutions of linear elasticity. The results have showed that the proposed method can be applicable to the analysis of kink deformation which had been observed experimentally in long-period stacking ordered magnesium alloy.
Keywords Computational Mechanics, Finite Deformation, Hyper-elasticity, Driving Force

1. Introduction

Magnesium alloys containing long-period stacking order (LPSO) phase have attracted a great deal of attention. The origins of both high strength and high ductility of these alloys are thought to be related to the grain refinement of matrix phase and kink deformation band of LPSO phase. Collective behaviors of dislocations on basal slip planes are important for the formation of kink deformation which consists of unique arrangement of microscopic lattice defects.

Theoretical studies of the relationship between lattice defect theory and generalized continuum theory have been carried out since early time, but they are still developping[4, 5, 6, 7].

There are quite a few literature of the deformation analysis using discrete dislocation plasticity and some disclination dynamics; e.g. deformation mechanism and mechanical properties[1], Interface crack[2], grain boundary[3], and so on.

However, there are few studies of formulation based on finite deformation except for Refs.[8, 9, 10]

In this study, the boundary value problem based on discrete defect theory is formulated to study the kink deformation using finite deformation theory. The essential mechanism of kink deformation is related to instabilities like buckling or localization of deformation. It will be important to consider the boundary value problem including lattice defects such as dislocations and disclinations.

2. Formulation

Some relative discontinuous displacement on planes $\partial\Gamma$ is considered in a hyper-elastic body Ω. Current coordinates for deformed position $\boldsymbol{x}$ is referred to the reference coordinates $\boldsymbol{X}$ for initial position, as shown in Fig.1. The displacement $\boldsymbol{u}$ is defined by $\boldsymbol{u} = \boldsymbol{x} - \boldsymbol{X}$. The tensors $\boldsymbol{F}$, $\boldsymbol{v}$, and $\boldsymbol{L} = \partial\boldsymbol{v}/\partial\boldsymbol{X}$

($\boldsymbol{l} = \partial \boldsymbol{v}/\partial \boldsymbol{x}$) are deformation gradient, velocity of a material point, and velocity gradient tensors, respectively An updated Lagrangian formulation is established.

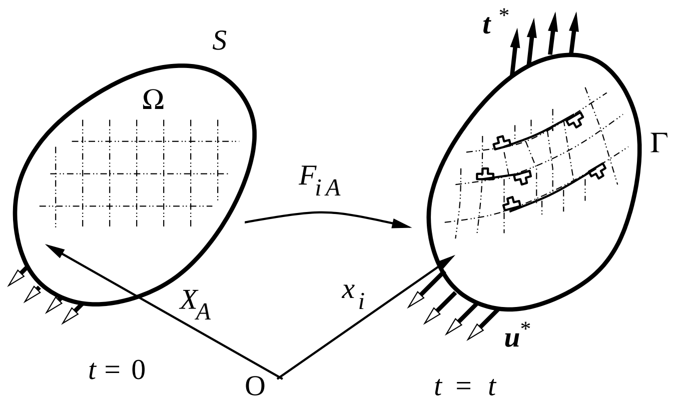

Figure 1. Boundary value problem of elastic body including discontinuous planes

2.1. Updated-Lagrangian Formulation

St.Venant-Kirchhoff material is assumed to be analyzed. The second Piola-Kirchhoff stress tensor $\boldsymbol{S}$ is expressed as a function of Green-Lagrange strain $\boldsymbol{E}$ as following:

$$S_{AB} = C^{(0)}_{ABCD} E_{CD} \tag{1}$$

where $\boldsymbol{C}^{(0)}$ is the elastic tensor. Truesdell's stress rate $\check{\boldsymbol{T}}$ is defined as follows:

$$\check{\boldsymbol{T}} = \dot{\boldsymbol{T}} - \boldsymbol{l}\boldsymbol{T} - \boldsymbol{T}\boldsymbol{l}^{\mathrm{T}} + \boldsymbol{T}\mathrm{tr}\boldsymbol{l}, \tag{2}$$

where $\boldsymbol{T}$ and $\dot{\boldsymbol{T}}$ are Cauchy stress tensor and its material derivative. Then, we assume the linearity between the Truesdell's stress rate $\check{\boldsymbol{T}}$ and strain rate tensor $\boldsymbol{d}$ with a tensor $\boldsymbol{C}$:

$$\check{T}_{ij} = C_{ijkl} d_{kl} \tag{3}$$

Using an approximation of the updated Lagrangian formulation, we obtain

$$C_{ijkl} = \frac{1}{J} F_{iA} F_{jB} F_{kC} F_{lD} C^{(0)}_{ABCD}. \tag{4}$$

where

$$J = \det|\boldsymbol{F}|. \tag{5}$$

For the UL formulation, the principle of virtual power is written as follows:

$$\int_{\Omega} \delta \boldsymbol{d}^T \mathbb{C} \boldsymbol{d} dv + \int_{\Omega} \delta \boldsymbol{l}^T \boldsymbol{T} \boldsymbol{l} dv = \int_{\Omega} \rho \dot{\boldsymbol{b}} \cdot \delta \boldsymbol{v} dv + \int_{\partial\Omega} \dot{\boldsymbol{t}}^* \cdot \delta \boldsymbol{v} da, \tag{6}$$

where ρ, $\dot{\boldsymbol{b}}$, and $\dot{\boldsymbol{t}}^*$ are mass density, body force, and surface traction, respectively.

2.2. Internal Discontinuous Deformation

The relative slip of $b\tau(t)$ on a slip plane $\partial\Gamma$ is described by

$$b\tau(t)M_A = X^+_A - X^-_A, \qquad \text{on } \partial\Gamma, \tag{7}$$

where M_A is the tangential vector along slip direction. $\boldsymbol{X}^+$ and $\boldsymbol{X}^-$ are the upper and lower reference coordinates on the slip plane at time t, respectively. b means the amount of unit discontinuous slip such as the norm of Burgers's vector. A monotonically increasing function $\tau(t)$ is varied from 0 to 1; $\tau(0) = 0$ and $\tau(t_{\text{end}}) = 1$, where t_{end} is the finish time. A linearized assumption of slip amount from $t = t^{(i)}$ to $t = t^{(i)} + \Delta t$ gives

$$b\tau(t^{(i)} + \Delta t) = b\tau(t^{(i)}) + b\dot{\tau}\Delta t, \tag{8}$$

where $\dot{\tau}$ means the temporal rate of τ. From Eq.(7),

$$b\tau(t^{(i)})M_A = (\boldsymbol{F}^{-1})^+_{Ai}x^+_i - (\boldsymbol{F}^{-1})^-_{Ai}x^-_i, \tag{9}$$

and

$$\begin{aligned} b\tau(t^{(i)} + \Delta t)M_A = &\left((\boldsymbol{F}^{-1})^+_{Ai} + (\boldsymbol{F}^{-1})^{+\bullet}_{Ai}\Delta t\right)(x^+_i + \dot{x}^+_i\Delta t) \\ &- \left((\boldsymbol{F}^{-1})^-_{Ai} + (\boldsymbol{F}^{-1})^{-\bullet}_{Ai}\Delta t\right)(x^-_i + \dot{x}^-_i\Delta t). \end{aligned} \tag{10}$$

Then, a rate type constraint condition is described by

$$b\dot{\tau}M_A - (\boldsymbol{F}^{-1})^+_{Ak}l^+_{ki}x^+_i - (\boldsymbol{F}^{-1})^-_{Ak}l^-_{ki}x^-_i - \left((\boldsymbol{F}^{-1})^+_{Ai}v^+_i - (\boldsymbol{F}^{-1})^-_{Ai}v^-_i\right) = 0, \tag{11}$$

and

$$b\dot{\tau}M_A - (\boldsymbol{F}^{-1})^+_{Ak}L^+_{kB}X^+_B - (\boldsymbol{F}^{-1})^-_{Ak}L^-_{kB}X^-_B - \left((\boldsymbol{F}^{-1})^+_{Ai}v^+_i - (\boldsymbol{F}^{-1})^-_{Ai}v^-_i\right) = 0, \tag{12}$$

in current coordinates system and in reference coordinates system, respectively. For the sake of simplicity in this study, we use the approximation as following

$$b\dot{\tau}\bar{F}_{iA}M_A - (v^+_i - v^-_i) = 0, \qquad \text{where} \quad \bar{F}_{iA} = F^+_{iA} + F^-_{iA}. \tag{13}$$

There are several approached for the computational setup. For example, the extended finite element formulation can be used as well as some cohesive zone model. In this study, we use the double nodes on the slip plane. A Lagrange multiplier λ_{L} is introduced to take into account the constraint condition (13), and the principle of virtual power (6) is modified as

$$\begin{aligned} &\int_\Omega \delta\boldsymbol{d}^T\mathbb{C}\boldsymbol{d}dv + \int_\Omega \delta\boldsymbol{l}^T\boldsymbol{T}\boldsymbol{l}dv + \int_{\partial\Gamma}\lambda_{\text{L}}\left(b\dot{\tau}\bar{\boldsymbol{F}}\boldsymbol{M} - (\boldsymbol{v}^+ - \boldsymbol{v}^-)\right)\cdot(\delta\boldsymbol{v}^+ - \delta\boldsymbol{v}^-)\,ds \\ &\quad = \int_\Omega \rho\dot{\boldsymbol{b}}\cdot\delta\boldsymbol{v}dv + \int_{\partial\Omega}\dot{\boldsymbol{t}}^*\cdot\delta\boldsymbol{v}da. \end{aligned} \tag{14}$$

3. Analysis Examples

3.1. Analysis Model

The isotropic hyper-elasticity model (St.Venant-Kirchhoff material) is used in the finite displacement assumption:

$$S_{AB} = C_{ABCD}E_{CD}, \quad C_{ABCD} = 2\mu\delta_{AC}\delta_{BD} + \lambda\delta_{AB}\delta_{CD}, \tag{15}$$

where $\boldsymbol{S}$ and $\boldsymbol{E}$ are the second Piola-Kirchhoff stress tensor and the Green-Lagrange strain. The parameter λ and μ are Lamé's constants. In this study, Poisson's ratio $\nu = \lambda/(2\lambda + 2\nu)$ is set to be 0.4.

Some results are compared with the analysis based on linear elasticity in the small displacement assumption:

$$T_{ij} = C_{ijkl}\varepsilon_{kl}, \quad C_{ijkl} = 2\mu\delta_{ik}\delta_{jl} + \lambda\delta_{ij}\delta_{kl}, \tag{16}$$

where $\boldsymbol{T}$ and ε is Cauchy stress tensor and small strain tensor, respectively.

Plane strain problems are assumed in a rectangular specimen of $100b \times 20b$, where b means the amount of unit discontinuous slip. The displacement on the left edge of the specimen is fixed and four different problems as shown in Fig. 2 are solved: Fig. 2(a) a dislocation dipole composed of two dislocations on 1-slip plane, (b) three dislocation dipoles on 3-slip planes, (c) some dislocation structures arranged on 3-slip planes, and (d) three dislocation dipoles on 3-slip planes under both compression and shear loading.

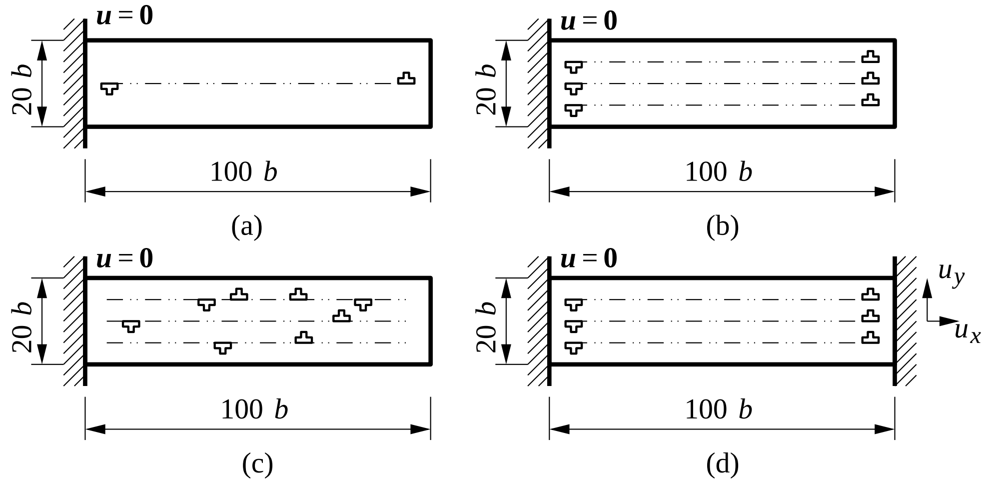

Figure 2. Schematics of model of analysis

3.2. Results of Analysis

3.2.1. Dislocation Dipoles on Slip Planes

Figure 3 shows the distribution of stress σ_{yy} on deformed body for (a) one dislocation dipole on 1-slip plane model, and for (b) three dislocation dipoles on 3-slip plane model. In Fig.3(a), the dislocation on the left affects a repulsive image force due to the fixed boundary condition. On the other hand, the dislocation on the right affects an attractive image force due to the traction-free boundary condition. According to the comparison between linear elasticity and hyper-elasticity models, both are almost same qualitatively.

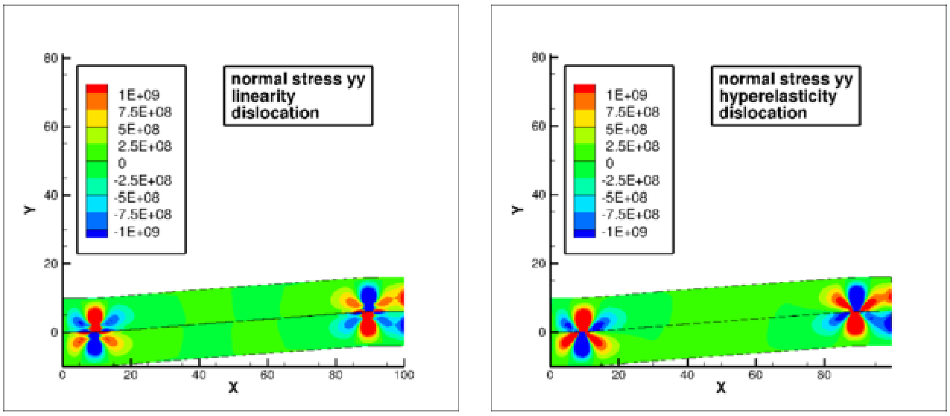

(i) linear elasticity model (ii) hyper-elasticity model

(a) 1-slip plane model

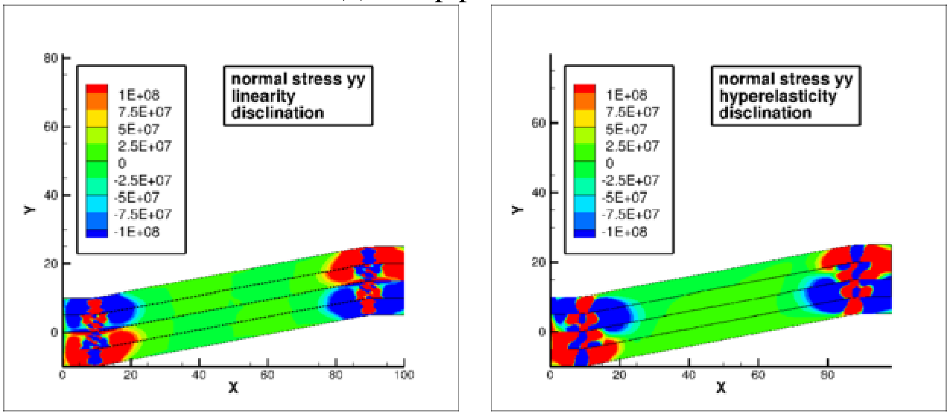

(i) linear elasticity model (ii) hyper-elasticity model

(b) 3-slip plane model

Figure 3. Distribution of stress σ_{yy} on deformed body

For the 3-slip plane model in Fig.3(b), the manners of image forces that act dislocations are similar to that for the 1-slip plane model in Fig.3(a). However, according to the comparison between linear elasticity and hyper-elasticity models, there appears some difference. The shape of stress contour has symmetry with respect to the neutral axis for the linear elasticity model. It is naturally understood, because the principle of superposition can be assumed in the small deformation theory. On the other hand, the shape of stress contour has non-symmetry with respect to the neutral axis for the hyper-elasticity model. This occurs due to the contribution of non-symmetric deformed shape of specimen.

3.2.2. Kink Deformation of Dislocations

The kink deformation in model 1 (Fig. 4(a)) and model 2 (Fig. 4(b)) corresponds to a wedge-type and ridge-type kink deformations, respectively. The deformation in model 3 (Fig. 4(c)) consists of two wedge-type kink deformation patterns. When the two edge dislocation array near the center of specimen merges to a dislocation wall on a single plane, model 3 is reduced to model 2. These types of kink deformation are often observed in zinc and LPSO magnesium alloy. The discrete dislocation plasticity based on finite deformation theory will be applicable to the investigation of such kink deformation mechanism.

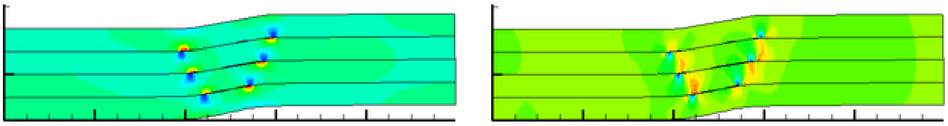

(i) σ_{xx} (ii) σ_{yy}

(a) model 1

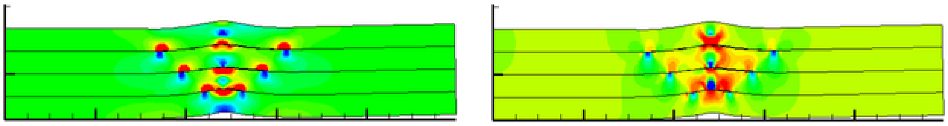

(i) σ_{xx} (ii) σ_{yy}

(a) model 2

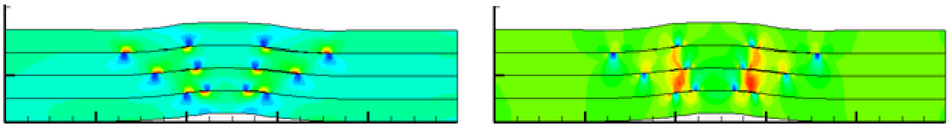

(i) σ_{xx} (ii) σ_{yy}

(a) model 3

Figure 4. Kink deformation expressed using discrete dislocations

3.2.3. Dislocation Dipoles on Slip Planes under Loading

Figure 5 shows the stress distribution σ_{xx} on deformed body for three dislocation dipoles on 3-slip plane model under both compression and shear loading. According to the comparison between (i) linear elasticity and (ii) hyper-elasticity models, deformed shape of specimens are similar to each other, but there appears some difference both qualitatively and quantitatively.

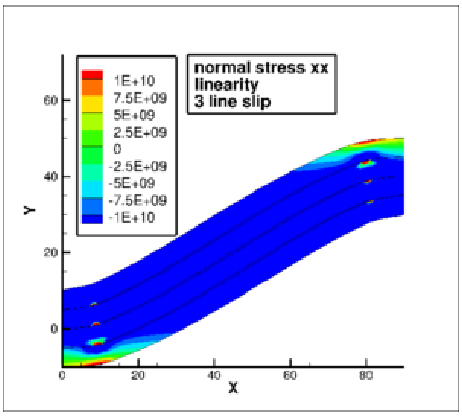

(i) linear elasticity model

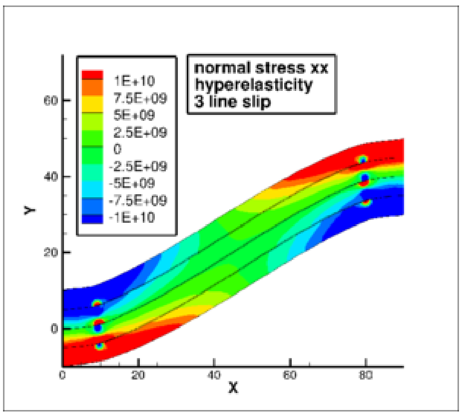

(ii) hyper-elasticity model

Figure 5. Distribution of stress σ_{xx} on deformed body under compression- shearing test

The stress contour for the linear elasticity model is simply recognized by the superposition of intrinsic stress field of dislocations and their image field, and external loading of compression and shearing. On the other hand, the typical bending stress due to the deformed shape of specimen can be observed in the shape of stress contour for the hyper-elasticity model.

4. Conclusions

An updated Lagrangian formulation based on finite deformation theory has been established for structural analysis of deformation of hyper-elastic body including lattice defects. A few examples have been shown for the application of the geometrically non-linear deformation of hyper-elastic body including lattice defects. The results have showed that the method can be applicable to the analysis of kink deformation which had been observed experimentally in long-period stacking ordered magnesium alloy. The criterion of dislocation nucleation, short-range interaction of lattice defects, and driving force of lattice defects should be discussed in the further study.

Acknowledgments

This work was supported by Grants-in-Aid for Scientific Research (KAKENHI).

References

[1] M. Seefeldt, Disclinations in Large-strain Plastic Deformation and Work-Hardening, Rev Adv Mat Sci 2 (2001) 44-79.
[2] A. Nakatani, W.J. Drugan, E. Van der Giessen, A. Needleman, Crack Tip Fields at a Ductile Single Crystal-Rigid Material Interface, Int J Fract 122 (2003) 131-159.
[3] V. Taupin, L. Capolungo, C. Fressengeas, A. Das, M. Upadhyay, Grain Boundary Modeling Using an Elasto-Plastic Theory of Dislocation and Disclination Fields, J Mech Phys Solids 61 (2013), 370-384.
[4] D.G.B. Edelen, A Gauge Theory of Dislocation and Disclinations, Springer-Verlag, Lecture Note in Physics, 1983.
[5] J.D. Clayton, D.L. McDowell, D.J. Bammann, Modeling dislocations and disclinations with finite micropolar elastoplasticity, Int J Plasticity 22 (2006) 210-256.
[6] M. Braun, Linear Elasticity with Couple Stresses, in: J.-F. Ganghoffer, F. Pastrone (eds.) Mech Microstru Solids 2, LNACM 50, Springer-Verlag Berlin Heidelberg 2010, pp.1-8.
[7] L. M. Zubov, Continuum Theory of Dislocations and Disclinations in Nonlinearly Elastic Micropolar Media, Mech Solids 46 (2008), 348-356.
[8] Leonid M. Zubov, Nonlinear Theory of Dislocations and Disclinations in Elastic Bodies, Springer, 1997.
[9] V.S. Deshpande, A. Needleman, E. Van der Giessen, Finite strain discrete dislocation plasticity, J Mech Phys Solids 51 (2003), 2057-2083.
[10] A. Acharya, C. Fressengeas, Coupled Phase Transformation and Plasticity as a Field Theory of Crystal Defects, Int J Fract 174, 87-94 (2012).